The vortex lattice of the type-II superconductor Nb studied by Small Angle Neutron Scattering (SANS)

Authors:
Dr. Jonathan White

SANS Beamline Practical

Laboratory for Neutron Scattering and Imaging

Paul Scherrer Institut

2020

Abstract

In this laboratory work we will study the vortex lattice (VL) of a type-II superconductor using Small Angle Neutron Scattering (SANS). The sample is a single crystal of Nb, an element with a superconducting critical temperature, $T_c = 9.3$ K and lower and upper critical fields of $H_{c1} = 0.18$T and $H_{c2} = 0.4$T, respectively. For external magnetic fields between H_{c1} and H_{c2} the superconductor is in the so-called intermediate state. In this state the magnetic field partially penetrates the material in the form of individual vortex lines that form a regular lattice, the vortex lattice (VL). This VL properties depend upon the microscopic superconducting state, and can be probed directly using the SANS technique. In this experiment we will study the behaviour of the VL as a function of the magnetic field.

1 Introduction

1.1 Superconductivity

A superconductor is a material that (i) conducts electrical current with no resistance ("perfect conductivity") and (ii) expels magnetic fields from its interior ("Meissner effect"). The property of perfect conductivity, or 'superconductivity', was first discovered in 1911 by the Dutch physicist Heike Kamerlingh Onnes. He observed that when a pure sample of elemental Hg was cooled below a critical temperature T_c of 4.2 K, the electrical resistance dropped suddenly to zero. In addition, to perfect conductivity and the Meissner effect, in the superconducting state no heat, sound or any other form of energy can be released from the material below T_c. The transition between the normal metal and superconducting states corresponds to a thermodynamic phase transition which can be observed as an anomaly in the thermal variation of the specific heat - see Figure 1 (a). As shown in Figure 1 (b) up to now, the superconducting transition occurs only at extremely low temperatures, well below room temperature. The discovery of a superconductor with T_c in the range of room temperature is a holy grail of modern Condensed Matter physics.

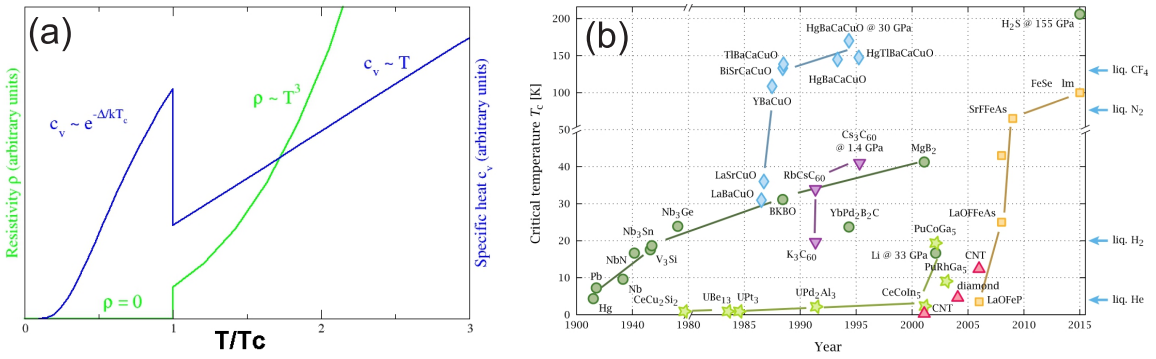

Figure 1: (a) Theoretical thermal variation of resistivity and heat capacity for the transition between the normal metal and superconducting states. (b) Time evolution over the last century of superconductivity in terms of discovered materials and critical temperatures. Both images from Ref. [1].

Of the known superconductors, there are two classes, type-I and type-II, which are distinguished experimentally according to their behaviour under an applied magnetic field. Figure 2 shows the ideal bulk magnetisation curves for both types, and the intrinsically

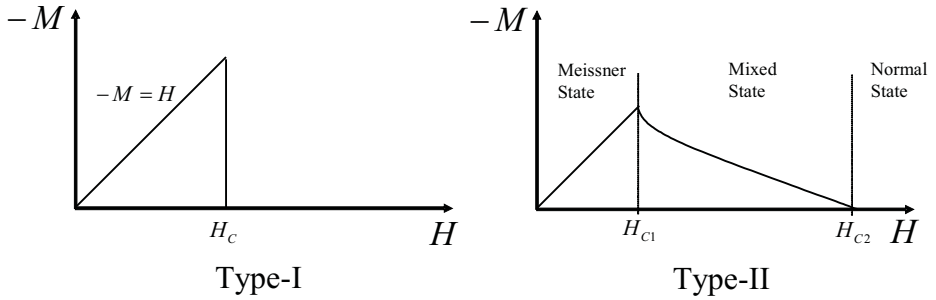

Figure 2: The magnetisation vs applied field curves for (a) a type-I superconductor and (b) a type-II superconductor. In a type II superconductor, and for an applied magnetic field above H_{C1}, the magnetic field penetrates the material in the form of vortex lines.

different behaviour. In type-I superconductors the magnetisation curve is characterised by the full Meissner effect, whereby there is an almost complete expulsion of internal fields from the bulk of the superconductor, except a penetration of the field into the surface over a characteristic length λ_L, called the London penetration depth. As $B = \mu_0(M + H)$, and $B = 0$ inside the bulk, the magnetisation follows $M = -H$. On increasing the field above a critical value H_c, the system undergoes a first-order transition into the normal state, where upon the superconducting state is destroyed.

Type-II superconductors possess two critical fields, the lower critical field, H_{C1} and the upper critical field, H_{C2}. Below H_{C1}, the sample exhibits the full Meissner state and behaves as if it were a type-I material. However, above H_{C1} the system becomes unstable to the admission of magnetic flux into the bulk and the magnetisation increases continuously as more flux enters the bulk on increasing the field. The magnetisation then becomes zero on passing through H_{C2}, typically undergoing a second-order transition into the normal state. The region between H_{C1} and H_{C2} is a distinct thermodynamic phase referred to as 'the mixed state,' wherein the VL exists.

The distinction between type-I and type-II superconductors is understood within the framework of Ginzburg–Landau (GL) theory [2]. This theory includes two key length-scales, the superconducting coherence length ξ (closely related to the amplitude of the GL superconducting order parameter $|\Psi|$), and λ_L. Generally for type-II superconductors, $\xi < \lambda_L$, and there is a negative interfacial energy between superconducting and normal regions. Here the system can minimise its energy by maximising the number of normal - superconducting interfaces, i.e. maximising the number of vortices (subject to limitations imposed by sample geometry and quantum mechanics). In contrast, for type-I superconductors where generally $\xi > \lambda_L$, the system is more stable with a minimal number of interfaces in the form of a single superconducting domain, i.e. no flux penetration and no vortex formation. The GL parameter $\kappa = \lambda_L/\xi$ is a useful parameter to identify if a superconductor is type-I or type-II. Strictly, superconductors with $\kappa < 1/\sqrt{2} \sim 0.707$ are type-I, while those with $\kappa > 1/\sqrt{2}$ are type-II [2].

The original theoretical work in the 1950s of A.A. Abrikosov was the first to show that the VL could be expected to exist in type-II superconductors [3]. For this insight he was awarded the Nobel prize in 2003, and vortices are often called 'Abrikosov' vortices in his honour.

1.2 The Vortex Lattice

The vortices in a type-II superconductor are quasi one-dimensional objects that can be visualised as lines of flux aligned with the direction of the applied magnetic field. The term 'vortex' refers to the vortical flow of spontaneous supercurrent that flows around the vortex core, and shields the rest of the superconducting state from the magnetic flux - see the black arrows Fig. 3(a). In the ideal case, vortices interact repulsively and arrange into a close-packed triangular VL. In real materials, this ordering scenario can be altered by either material inhomogeneities that pin the vortex lines, thermal fluctuations close to T_c that cause the VL to 'melt', or intrinsically anisotropic properties of the superconductor itself. Thus by studying the VL structure and coordination, insights into the physics of the host material can be obtained.

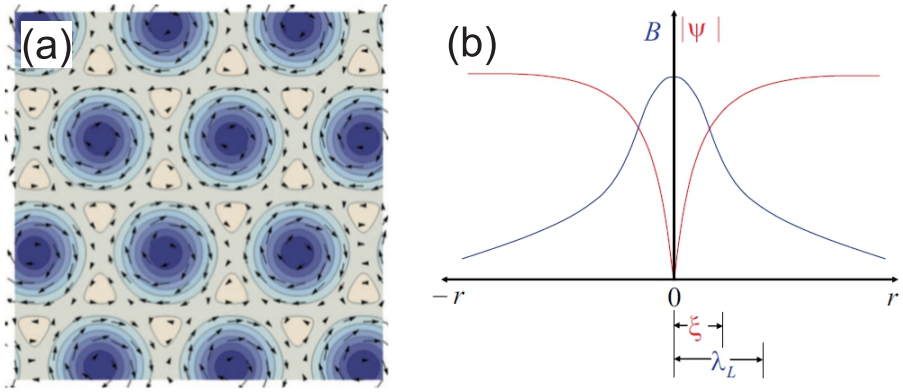

Figure 3: (a) A top view of a triangular VL with applied field into the page (arrows indicate directions of the superflow). The colour scale denotes the relative amplitude of the flux density; a darker blue indicates a higher magnetic flux density. (b) A schematic picture of a single vortex, with the dependencies of internal field and GL order parameter magnitude on distance from the vortex core. Characteristic length-scales ξ and λ_L are also noted.

Conveniently, quantum mechanics dictates each vortex line in *any* type-II superconductor to carry exactly one magnetic flux quantum $\Phi_0 = h/(2e) = 2.067 \cdot 10^{-15}$ Wb. This also corresponds to the total flux in each VL unit cell. By increasing the applied magnetic field, the vortex density increases and scales proportionally with the applied magnetic field. It can shown that the minimum distance d between VL planes is given by:

$$d = \sqrt{\frac{\Phi_0}{B}\sigma}, \tag{1}$$

where B is the internal field (usually taken to be same as the applied field), Φ_0 is the flux quantum and $\sigma = \sin\beta$ is a dimensional constant that depends on the VL coordination. For a triangular VL, $\beta = 60°$ and $\sigma = \sqrt{3}/2$, while for a square VL $\beta = 90°$ and $\sigma = 1$. Table 1 shows some calculated d values for a perfectly triangular VL as a function of internal field, B.

Importantly for what follows, the scattering of neutrons by the VL is elastic and described by Bragg's Law:

$$\lambda_n = 2d\sin(\theta), \tag{2}$$

Table 1: Shortest distance between planes for a perfectly triangular VL.

B (T)	d (Å)
0.2	946
0.3	772
0.4	669

where λ_n is the neutron wavelength, d is the plane-spacing of the VL (given in Table 1) and θ is the Bragg angle.

2 Neutron Scattering

The most prominent scattering techniques in material research use photons, electrons or neutrons. Owing to the different properties of the scattered particle, i.e. charge, spin, mass and energy, one often selects a combination of the complementary scattering techniques to obtain a complete understanding of the investigated problem.

The neutron was discovered in the UK by J. Chadwick in 1932, while the first high-flux neutron diffraction experiments were performed and developed in the USA by E.O. Wollan and C. Shull in 1945-1946. Each of these activities were recognised with Nobel prizes in 1935 and 1994, respectively. The properties of the neutron make them very suitable for Condensed Matter research: as shown in Table 2 they are electrically neutral, and hence they penetrate matter more deeply than electrically charged particles of comparable kinetic energy. Being uncharged makes neutrons a valuable probe, since not only do they easily penetrate the bulk of the investigated material, but also bulky experimental equipment, e.g., cryostats, magnets or pressure cells. This advantage also has a downside; the weak interaction between the neutrons and the nuclei of the scatterer leads to a low number of scattering events. Therefore, relatively high incident neutron fluxes and long counting times are unavoidable, for example, when compared with x-ray scattering.

Table 2: Physical Properties of the neutron

mass m_n	1.674110^{-27} kg
charge	0
spin	1/2
magnetic dipole moment μ	$-1.913\mu_N$
free neutron life time τ	881.5 s
de Broglie wavelength λ	$\frac{h}{m_n v}$
kinetic energy E	$\frac{m_n v^2}{2} = \frac{m_n}{2}(\frac{h}{\lambda})^2$

Free neutrons can be produced by either fission in nuclear reactors, or spallation at accelerator-based sources, and then moderated to the required energy. A portion of the neutrons produced can be directed to the sample of interest using neutron guides, which use 'supermirrors' and the principle of total reflection for the neutron. The energy of

neutrons with a wavelength of order interatomic distances matches very well the typical energies of lattice and spin excitations in solids. This makes neutron scattering particularly suitable for investigations of static structures and dynamic processes in Condensed Matter.

Crucially, neutrons carry a spin $S = 1/2$ and a significant magnetic moment. The interaction between the neutron magnetic moment and local field variations inside a solid can cause the neutrons to both scatter elastically and inelastically. This makes them insightful probes of ordered magnetic structures and excitations, and importantly for us here, the local internal field variation due to the VL in type-II superconductors.

Table 3: Wavelength, frequency, velocity, and energy relationship for neutrons

Quantity	Relationship	Value at 2 meV
Energy	$[\text{meV}] = 2.072k^2[\mathring{A}^{-1}]$	2 meV
Wavelength	$\lambda[\mathring{A}] = \frac{9.044}{\sqrt{(E[meV])}}$	6.4 $[\mathring{A}]$
Wave vector	$k[\mathring{A}^{-1}] = \frac{2\pi}{\lambda[A]}$	0.982 $\mathring{A}^{-1}$
Frequency	$\nu[THz] = 0.2418E[meV]$	0.484 THz
Wavenumber	$\nu[cm^{-1}] = \nu[Hz]/(2.99810^{10}cm/s)$	16.1 cm^{-1}
Velocity	$\text{v[Km/s]} = 0.632\text{k}[\ \mathring{A}^{-1}]$	0.62 Km/s
Temperature	$T[K] = 11.605E[meV]$	23.2 K

2.1 Neutron Sources

The neutrons used in scattering experiments can be obtained from a nuclear reactor, like the high flux reactors at Oak Ridge National Laboratory (ORNL) at Oak Ridge in the USA, and at the Institute Laue-Langevin (ILL) in Grenoble, France, or the FRM-II reactor in Garching near Munich, Germany. Here the neutrons are produced by spontaneous fission of ^{235}U. Typically 'thermal' neutrons with a Maxwellian energy spectrum peaked around 320 K ($\lambda \sim 1.7$ Å) are produced. By moderating these neutrons to temperatures in the range 20 K to 40 K, 'cold' neutrons can be obtained with a spectrum peaked around $\lambda \sim 6$ Å. Research reactors work in the same way as nuclear power stations but are designed so that a high neutron flux can exit the moderator system for use in research.

There are also neutron spallation sources like Swiss spallation source, SINQ at PSI, where neutrons are produced upon bombarding heavy nuclei (like U, W, Ta, Pb or Hg) with high-energy protons. Here the bombardment by protons bring the target nuclei into an excited state, such that neutrons 'evaporate 'from the target. These neutrons are moderated in the same way as in a reactor to obtain a thermal or cold spectrum of neutrons for scattering experiments. Most spallation sources such as ISIS in the UK, or the Spallation Neutron Source (SNS), at ORNL, USA, are pulsed sources, delivering intense pulses of neutron radiation. SINQ is an exception to this since a near-continuous neutron beam is produced. A new European Spallation Source (ESS) is being built in Lund, Sweden. It will become operational in 2019 and it is expected to be the new flagship European neutron science facility.

2.2 Reciprocal space and scattering diagram

The laws of momentum and energy conservation governing all scattering experiments are:

$$\begin{aligned} \mathbf{Q} &= \mathbf{k_f} - \mathbf{k_i}, \\ |\mathbf{Q}| &= \mathbf{k_i^2} + \mathbf{k_f^2} - 2|\mathbf{k_i}||\mathbf{k_f}|cos(\theta_s), \\ \hbar\omega &= E_i - E_f \end{aligned}$$

Here the magnitude of the neutron wave vector is $k = 2\pi\lambda$, where λ is the neutron wavelength, while its momentum transfer $\mathbf{Q}$. Subscripts i, f refer to the incident and final (scattered) neutron state. The angle between the incident and final beams is $2\theta_s$ and the energy transferred to the sample is $\hbar\omega$. Due to the finite mass of the neutron, its dispersion relation is

$$\begin{aligned} E &= \frac{\hbar^2 k^2}{2m_n} \\ E[meV] &= 2.072k^2[\mathring{A}^{-1}] \\ \hbar\omega &= \frac{\hbar^2 k^2}{2m_n}(ki^2 - k_f^2) \end{aligned}$$

In any scattering experiment one measures the incident (i) and and final (f) neutron beams, and deduces any energy or momentum transfer between the neutron and the sample. For elastic neutron scattering $|k_i| = |k_f|$. To understand better the elastic scattering process, Fig. 4 (a) shows a simple reciprocal lattice for a two-dimensional crystalline solid where each point corresponds to a reciprocal lattice point. The circle is a 2D representation of the diffraction sphere ('Ewald' sphere) which describes allowed elastic scattering processes. This circle has a radius k, and its origin is termed the 'origin of diffraction'. The incoming and outgoing neutron wave vectors originate from this point. Wave vector k_i connects the origin of diffraction to the origin of reciprocal space (also a reciprocal lattice point), while k_f connects the origin of diffraction to the reciprocal lattice point of interest. When the ends of k_i and k_f span a cord of the diffraction circle, the length of the cord is $\mathbf{Q}$, and diffraction intensity can be observed experimentally. Different directions of k_f are reached experimentally by rotating the sample and/or detector so that this 'Bragg condition' is satisfied.

Fig. 4 (b) shows the case for neutron diffraction from the VL, which itself forms a 2D reciprocal lattice in the plane perpendicular to the applied magnetic field. Here the Ewald sphere is shown in grey, and the incoming wave vector (denoted $\mathbf{k}$) is parallel to the direction of the field. In the diagram, the reciprocal lattice (or the sample) has been rotated by an angle of ω, such that the Ewald sphere touches two points of the reciprocal lattice at $\mathbf{k}$ and $\mathbf{k'}$. Here momentum conservation is satisfied and a Bragg spot can be observed on the detector. Without the reciprocal lattice rotation, the Ewald sphere touches the reciprocal lattice at only one point (the origin of reciprocal space), and momentum conservation is not satisfied, and no diffraction peaks are observed.

At the diffraction condition [Fig. 4 (b)], the angle between $\mathbf{k}$ and $\mathbf{k'}$ is given by 2θ, which is of the order of 1 °. Since the detector is fixed in space, we rotate (or 'rock') the sample and magnet together over a small angular range, i.e. we scan for Bragg spots by rocking

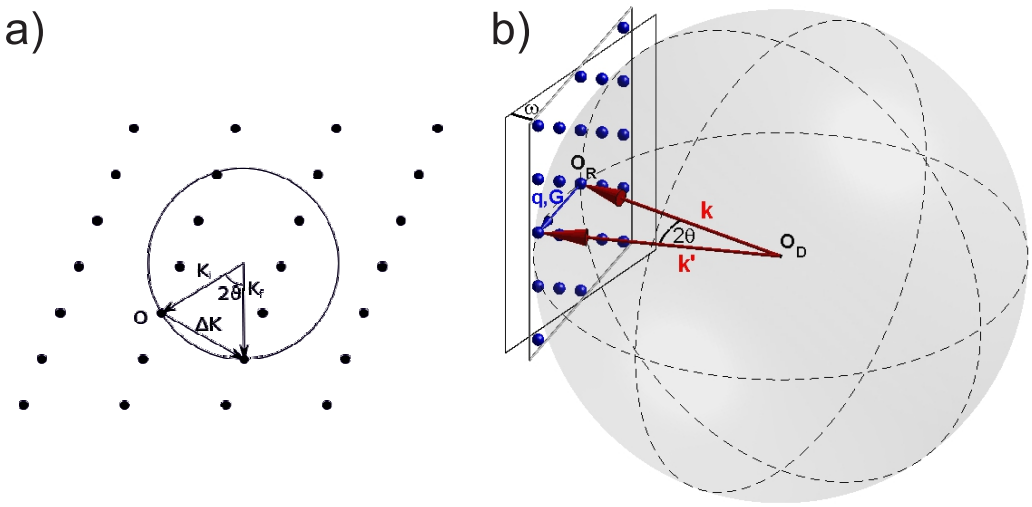

Figure 4: (a) A diffraction diagram using Ewald sphere (circle) construction. (b) Schematic of the Ewald Sphere for neutron diffraction from a VL in a type-II superconductor. The reciprocal VL points are shown by blue spheres, and it has been rotated by an angle ω such that the Bragg diffraction condition is satisfied.

scans. Since we always detect scattering at angles less than 3°, we justify the nomenclature of small angle scattering. Such diffraction signals at low angles cannot be detected with conventional neutron diffraction instruments that are usually designed to measure Bragg peaks at scattering angles above 10°.

2.3 Scattering from the vortex lattice

Due to the intrinsic magnetic dipole moment of the neutron, it may interact with spatially-varying local magnetic fields $\mathbf{B(r)}$ due to the VL inside a type-II superconductor. The scattering potential is simply given by

$$V = -\gamma\mu_N \mathbf{B}(\mathbf{r}) \tag{3}$$

where $\gamma = 1.91$ is a dimensionless constant, μ_N is the nuclear magneton and $\mathbf{B(r)}$ is the field distribution of the VL. For an applied field aligned with the nominal z-direction, $\mathbf{B}$ = (0, 0, B), as expected for the ideal VL, and the elastic differential cross-section for magnetic scattering becomes

$$\frac{d\sigma}{d\Omega} = \left(\frac{m_n}{2\pi\hbar^2}\right)^2 \gamma^2\mu_N^2 \left|\int B(\mathbf{r})\exp(i\mathbf{q}\cdot\mathbf{r})d\mathbf{r}\right|^2 S(\mathbf{q}) \tag{4}$$

where m_n is the neutron mass, and $S(\mathbf{q})$ is the structure factor which describes that the neutrons are scattered by a periodic potential of a 2D lattice. We have also introduced $\mathbf{q} = \mathbf{k} - \mathbf{k}'$ with $\mathbf{q}$ being the scattering vector. Since the reciprocal VL can be described in terms of a primitive basis, individual scattering vectors are labelled $\mathbf{q_{h,k}}$, with indices h and k. Note that *any* reciprocal VL can be constructed using just two basis vectors that can be denoted $\mathbf{q_{1,0}}$ and $\mathbf{q_{0,1}}$.

The final expression for the integrated intensity $I(\mathbf{q_{h,k}})$ of a VL Bragg spot of order h, k can be written as:

$$I(\mathbf{q_{h,k}}) = 2\pi V \phi_n \left(\frac{\gamma}{4}\right)^2 \frac{\lambda_n^2}{\Phi_0^2 q_{h,k} \cos(\zeta)} |F(\mathbf{q_{h,k}})|^2 \tag{5}$$

where ϕ_n is the neutron flux per unit area, V is the illuminated volume of the sample, λ_n is the neutron wavelength and $\cos(\zeta)$ is the Lorentz-factor. The angle ζ is that which lies between the reciprocal lattice vector and the direction normal to the rotation axis. $F(\mathbf{q_{h,k}})$ is the so-called VL form factor, defined as the 2D Fourier transform of the field-distribution for the VL unit cell (the modulus quantity in Equation (4)). By determining the quantity $I(\mathbf{q_{h,k}})$ experimentally, we can obtain the quantity $|F(\mathbf{q_{h,k}})|$ which can then be compared with model expectations for the internal field-distribution of the VL.

A commonly used model for $|F(\mathbf{q_{h,k}})|$ is the so-called (modified) London model [8]:

$$F(\mathbf{q_{h,k}}) = \frac{\langle B \rangle \exp(-0.44 q_{h,k}^2 \xi^2)}{1 + q_{h,k}^2 \lambda_L^2}. \tag{6}$$

Here B is the applied magnetic field, and $q_{h,k}$ is the field dependent reciprocal lattice vector. By measuring the magnetic field dependence of of the VL form factor, it is possible to extract important superconducting properties of Nb: the London penetration depth λ_L and and the Ginzburg-Landau coherence length ξ.

2.4 Rocking-curve measurements

As mentioned in Section 2.2, as in any diffraction experiment the key information obtained from SANS measurements on the VL is obtained from rocking-curve measurements. Formally this requires rotating the sample and thus a reciprocal lattice vector through the Bragg condition at the detector, and recording the diffracted intensity as a function of rotation (rocking) angle. Due to the small angles involved, it is important to carefully align the sample with respect to both the magnetic field and neutron beam before rotating the reciprocal lattice.

To perform a rocking scan, you must choose a range of angles over which to rotate the reciprocal lattice and measure the diffracted intensity. Typically this range has the expected Bragg angle at the midpoint. Ideally the angular range should take into account the anticipated angular width of the rocking curve as might be expected from resolution considerations, and be wide enough so that at the widest scanned angles the observed intensity falls to the background level.

In SANS experiments, there are two activities required to record the rocking curve of a Bragg spot. The first is clearly to perform the measurement of the VL scattering, while the second is to perform background measurements with no VL established in the sample (above $T_c(H)$, or after zero-field cooling). The background data are then subtracted from 'foreground' data (where the VL is present), leaving just the diffracted signal from the VL.

3 SANS Spectrometer

A classical SANS instrument has a pinhole geometry, as shown in Fig. 5. A polychromatic, 'white'neutron beam is guided to the instrument from the neutron source, and a

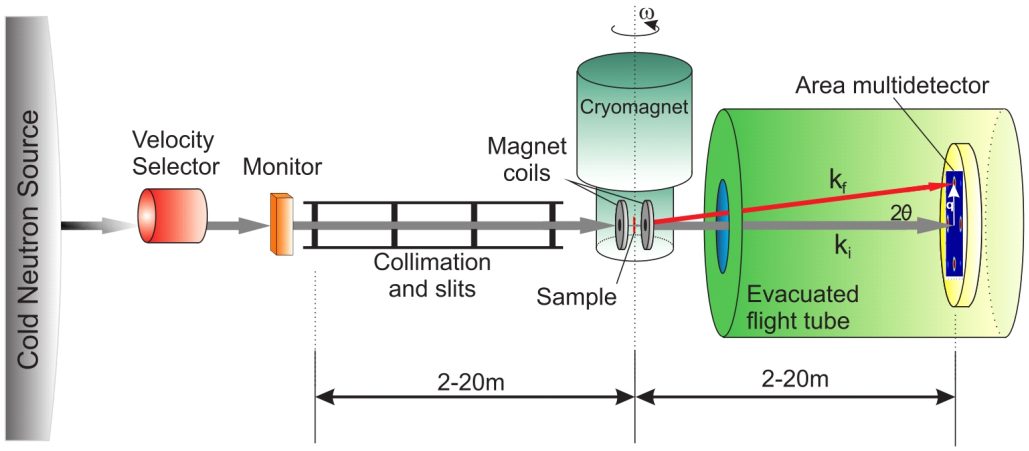

Figure 5: A schematic diagram of a typical SANS instrument. In the usual pinhole geometry, the length of the collimator section is approximately equal to the distance between the sample and the area multidetector. Each distance can be up to 18 m on the SANS-I instrument. Shorter distances are used as the momentum transfer increases.

monochromatic beam is generated by selecting a narrow range of wavelengths with a mechanical neutron velocity selector. Typically, the FWHM of the wavelength distribution of the monochromatic beam is 10% of its peak position. The beam profile is then controlled using pinholes placed in a collimation section of the instrument before it is incident on the sample. Scattered neutrons are counted with an area sensitive detector located at some variable distance from the sample. Usually, the flight path from sample to detector has the same length as the collimation section, as this configuration gives the optimal compromise for beam intensity and resolution. A typical SANS detector is a ^{3}He detector with an area $\sim$ 1 m^2 and 128 x 128 pixels. The pixelated detector provides a spatial resolution that allows the determination of the scattering angle 2θ of the counted neutrons and the corresponding momentum transfer $q = (4\pi/\lambda_n)\sin(\theta/2)$. The SANS setup outlined above is typical for continuous neutron sources. Modern SANS instruments offer different sample environments for experiments under tailored conditions with e.g. controlled temperature, applied pressure, electric or magnetic fields, or controlled humidity.

4 Data Reduction and Analysis

To analyze the VL signal observed on the detector, data measured in the superconducting phase (foreground) have data taken above T_C (background) subtracted, whereby each dataset is measured for identical conditions of the instrument, such as incident neutron wavelength λ_n, collimation, detector distance, slits and the same rocking angles. To obtain reproducible results, the intensity data are normalized to a standard counting monitor.

Fast data visualization and analysis can be carried out using the GRASP software developed by C.D. Dewhurst at the ILL [7]. The software is developed within a Matlab environment, and as such it can handle the two-dimensional and pixelated multidetector data recorded by the SANS instrument. The user interface includes a window that allows a view of the distribution of the diffracted intensity across the multidetector at a certain rotation angle of the reciprocal lattice. It is also possible to sum the measurements at

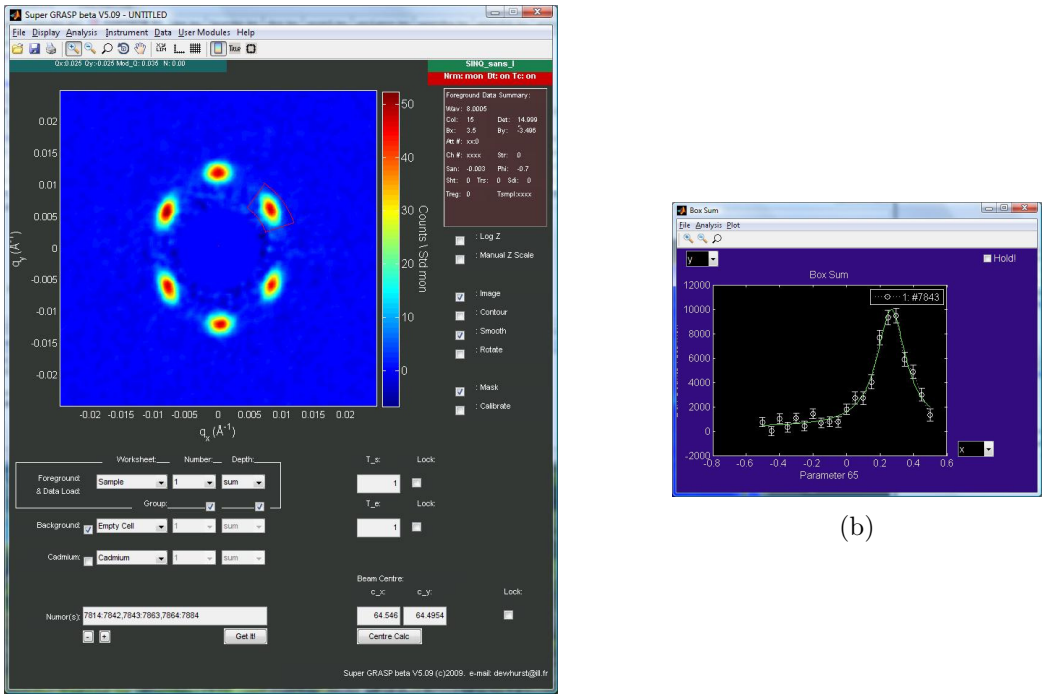

(a) (b)

Figure 6: (a) Image capture of the front-end of the GRASP software (version 5.09). SANS data over multiple rocking curves is loaded, showing all the first-order Bragg spots in a single image. A sector box is defined on the detector over area occupied by the upper right Bragg spot. (b) Image capture of a rocking curve plot output by the GRASP software, and fit with a suitable lineshape function. The horizontal axis is in units of degrees of rotation angle of the reciprocal lattice about the vertical axis, where zero corresponds to the straight through position. The vertical axis is in units of total counts within the sector box per standard monitor.

many rotation angles together into just one image, providing a picture of the diffracted intensity over an entire rocking curve. By similarly summing over multiple rocking curves, it is possible to deduce the VL coordination by showing all of the first-order Bragg spots in just one image.

To perform the data analysis one uses the GRASP front panel. One may, for instance, add SANS foreground data summed over numerous rocking curves. The corresponding background data can also be properly subtracted leaving angle-dependent VL rocking scan data that are properly normalized. Statistical noise that occurs close to the beam stop can be easily masked.

In Fig. 6a we show an image capture of the front-end of the GRASP software. SANS data over multiple rocking curves is loaded, showing all the first-order Bragg spots in a single image. A sector box is defined on the detector over area occupied by the upper right Bragg spot. In Fig. 6 we show an image capture of a rocking curve plot output by the GRASP software, and fit with a suitable lineshape function. The horizontal axis is in units of degrees of rotation angle of the reciprocal lattice about the vertical axis, where zero corresponds to the straight through position. The vertical axis is in units of total counts

within the sector box per standard monitor. From the fit of the data we obtain $I(\mathbf{q_{h,k}})$, and then the quantity $|F(\mathbf{q_{h,k}})|$ can be determined.

5 Experimental Procedure

1. Before the experiment, estimate the reciprocal lattice vectors ($q_{1,0}$ and $q_{0,1}$) for a perfect hexagonal VL and for various applied fields, between 0.18 and 0.4T.

2. For the same fields determine the scattering angles 2θ between the incident and final neutron beam.

3. You will be given a Nb single crystalline sample. Measure its dimensions and mass. The sample will be surrounded by Cd that will determine the illuminated area.

4. Mount the Nb sample in a sample holder, insert it into the cryo-magnet (MA11) and start cooling the system.

5. Use a neutron camera to verify that the sample is in position (i.e., at the centre of the neutron beam).

6. Configure the instrument correctly and adjust the beam stop, which is intended to block the direct beam to protect the detector.

7. Measure the position and transmission of the direct beam by placing an attenuator in the beam and removing the beamstop.

8. Cool the system to 10 K, above T_c, and perform rocking scans as background measurements.

9. Apply fields between 0.18 and 0.4 T and in each case each field cool through T_c down to the lowest temperature, 1.8 K.

10. Perform foreground measurements (the same scans as in the background).

11. Use GRASP to make sets of foreground - background signals. Sum all the data (with the background subtracted) and measure the opening angles between the Bragg spots to determine the symmetry of the reciprocal VL.

12. Use GRASP to make plots of intensity vs. rocking angle. Determine the position and width of the Bragg peaks, and fit with a lineshape to obtain $I(\mathbf{q_{h,k}})$.

13. If time: From the integrated intensity data calculate the form factor as a function of applied field.

14. If time: Fit the form factor data with the modified London model and extract both the low temperature estimates for the London penetration depth of Nb and the Ginzburg-Landau coherence length. From these results determine the κ parameter for Nb. The typical value of κ for Nb varies with sample purity, but is usually ~ 0.71. How does your value compare? Why might there be a discrepancy?

More information of the instrument is available at our web page
http://www.psi.ch/sinq/sansi/sans-i
The description of the program running the experiment, SICS, is described at
http://www.psi.ch/sinq/sansi/manuals.

References

[1] https://en.wikipedia.org/wiki/Superconductivity

[2] Lifshitz, E. M. and Pitaevskii, L. P. Statistical Physics. Oxford: Pergamom, (1980).

[3] A.A. Abrikosov, Sov. Phys. JETP **5**, 1174 (1957).

[4] C. G. Windsor. *An introduction to small-angle neutron scattering.* J. Appl. Cryst., **21**,582, 1988.

[5] G. L. Squires. *Introduction to the theory of thermal neutron scattering.* Cambridge University Press, Cambridge, 1978.

[6] J. Kohlbrecher and W. Wagner, Appl. Cryst. **33**, 804 (2000).

[7] C. D. Dewhurst, GRASP User Manual, Technical Report No. ILL03DE01T, Institut Laue-Langevin, Grenoble, 2003, available at [http://www.ill.fr/lss/grasp].

[8] A. Yaouanc, P. Dalmas de Réotier, and E. H. Brandt, Phys. Rev. B **55**, 11107 (1997).